THE GEOLOGICAL SOCIETY OF AMERICA®

Discovery of Upper Cretaceous Neo-Tethyan trench deposits in south Tibet (Luogangcuo Formation)

Wei An[1,2,*], Xiumian Hu[2,*], and Eduardo Garzanti[3,*]

[1]SCHOOL OF RESOURCES AND ENVIRONMENTAL ENGINEERING, HEFEI UNIVERSITY OF TECHNOLOGY, HEFEI, 230009, CHINA
[2]STATE KEY LABORATORY OF MINERAL DEPOSITS RESEARCH, SCHOOL OF EARTH SCIENCES AND ENGINEERING, NANJING UNIVERSITY, NANJING, 210023, CHINA
[3]DEPARTMENT OF EARTH AND ENVIRONMENTAL SCIENCES, UNIVERSITÀ DI MILANO-BICOCCA, MILANO, 20126, ITALY

ABSTRACT

Sedimentary basins within the Transhimalayan arc-trench system provide paleotectonic and paleogeographic information on the evolution of the late Mesozoic–early Cenozoic Neo-Tethyan subduction zone along the southern Asian margin. This paper presents detailed stratigraphic, sedimentologic, petrographic, detrital-zircon geochronologic and Hf isotopic data from the Luogangcuo Formation exposed as part of the Xiukang Mélange in south Tibet. The Luogangcuo Formation was deposited (ca. 88–81 Ma) in a trench environment on a deep-sea fan fed from the Lhasa block through a submarine canyon. Dominant chert and subordinate sandstone and limestone clasts in conglomerate beds indicate recycling from the Neo-Tethyan subduction complex during repeated episodes of gravitational failure. The interbedded turbiditic sandstones were sourced directly from the Gangdese magmatic arc and central Lhasa terrane. Detrital volumes from the active Asian margin increased markedly at ca. 88 Ma as a result of uplift of central Lhasa, leading to deltaic progradation, filling of the Xigaze forearc basin, and bypassing of sediments funneled via canyons across the subduction complex to reach the Luogangcuo trench basin at abyssal depths.

LITHOSPHERE; v. 10; no. 3; p. 446–459; GSA Data Repository Item 2018140 | Published online 23 March 2018 https://doi.org/10.1130/L690.1

INTRODUCTION

The subduction of oceanic lithospheric slabs is one of the extraordinary plate-tectonic processes that recycles crustal material in the mantle, leads to crustal growth, and determines prominent changes in the topography of continental margins (e.g., Armstrong, 1991; Scholl and von Huene, 2007; Flament et al., 2015). During subduction of oceanic lithosphere, an arc-trench system develops on the upper plate, including a trench, a subduction complex, a forearc basin, and a magmatic arc (Dickinson, 1995). Sedimentary basins form in different positions within the arc-trench system, at the trench, perched on top of the subduction complex, and along the forearc region (Busby and Ingersoll, 1995). They represent an archive of detritus with varied composition from which paleotectonic and paleogeographic information on the evolution of the subduction system (sediment-dispersal patterns and source-to-sink relationships, submarine topography, uplift and erosional history of the active margin) can be retrieved via provenance analysis (Dickinson, 1995; Underwood and Moore, 1995).

As one of the best preserved suture zones on Earth, the Yarlung-Zangbo suture of the Himalaya (Fig. 1A) marks the site of late Mesozoic Neo-Tethyan subduction (e.g., Searle et al., 1987; Yin and Harrison, 2000) and subsequent India-Asia collision at ca. 59 Ma (DeCelles et al., 2014; Wu et al., 2014; Hu et al., 2015, 2016, 2017). The complete process of oceanic subduction followed by continent-continent collision is documented. In the last decades, the Himalayan suture zone has been consequently recognized as the unexcelled natural laboratory to study subduction and collision (Tapponnier et al., 1981; Allègre et al., 1984; Dewey et al., 1988; Matte et al., 1997; Hodges, 2000; Yin and Harrison, 2000). The Neo-Tethyan arc-trench system in south Tibet includes trench and trench-slope deposits as thrust sheets or blocks, the subduction complex, and the extensively studied Xigaze forearc basin and Gangdese magmatic arc (Fig. 1B) (Einsele et al., 1994; Dürr, 1996; Dupuis et al., 2005, 2006; Ji et al., 2009; Wu et al., 2010; Aitchison et al., 2011; Cai et al., 2012; Wang et al., 2012; An et al., 2014, 2017). Notably less has been done to identify trench deposits, with the exception of the Nindam Formation in the Ladakh Himalaya, India (Garzanti and Van Haver, 1988) and the Rongmawa Formation in Ngamring, south Tibet (Cai et al., 2012). This may be ascribed to poor preservation owing to strong multiple deformation during tectonic accretion and final collision, and to much smaller size and only local exposure relative to the thick and well preserved forearc-basin successions. Studies of trench deposits identified along the Neo-Tethyan suture zone are nevertheless essential to provide paleogeographic information and reconstruct the uplift and erosion history of the Asian active margin, and to allow comparison with other trench basins worldwide.

We present here new stratigraphic, sedimentological, petrographic, and U-Pb geochronology and Hf isotope data on detrital zircons from an ~200-m-thick succession of conglomerates and sandstones exposed within the Yarlung-Zangbo suture zone of south Tibet. Such evidence suggests that the unit, first identified here under the name Luogangcuo Formation, was deposited in the Neo-Tethyan trench basin. This study thus adds a new element for an accurate reconstruction of the Asian active margin of Neo-Tethys during the Late Cretaceous.

GEOLOGICAL SETTING

The Tibetan Plateau formed through the successive accretion of Gondwana-derived terranes to Asia, the latest of which being the Paleocene collision of India with the Lhasa block representing the southern margin

*Corresponding author, An: anwei@hfut.edu.cn; Hu—huxm@nju.edu.cn; Garzanti—eduardo.garzanti@unimib.it.

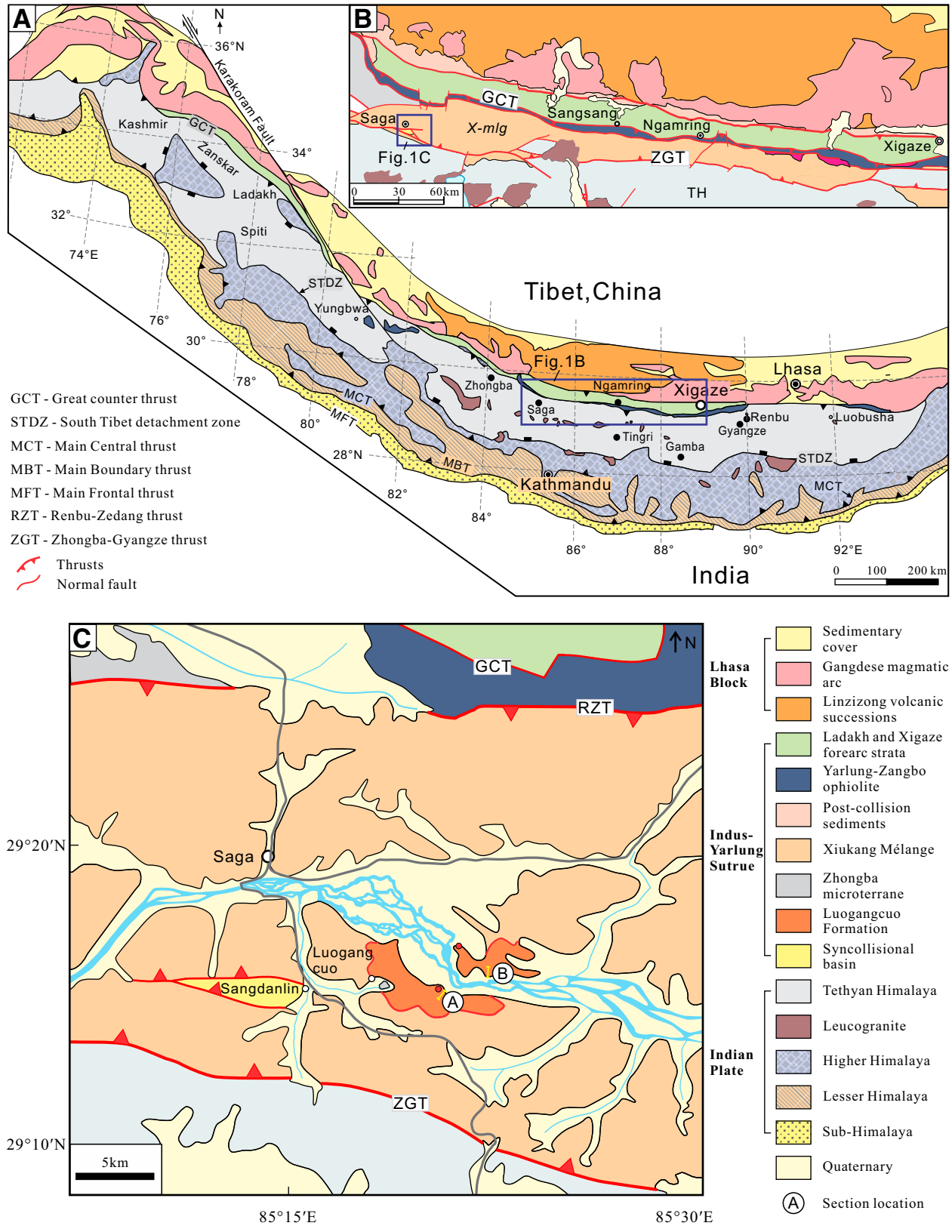

Figure 1. (A) Geological map of the Himalaya and southern Tibet (after Yin, 2006). (B) Geological map of the Saga-Xigaze area (after Pan et al., 2004). (C) Detailed map of the Saga area (modified after Wang et al., 2011, and Li et al., 2007).

of Asia (e.g., Allégre et al., 1984; Dewey et al., 1988; Yin and Harrison, 2000; Wang et al., 2011; DeCelles et al., 2014; Hu et al., 2015). The Lhasa block is subdivided into northern, central, and southern terranes characterized by different magmatic and sedimentary units (Zhu et al., 2011). The northern Lhasa terrane is characterized by a mainly Jurassic-Cretaceous sedimentary succession and Cretaceous igneous rocks (Zhu et al., 2011). The central Lhasa terrane consists of widespread Permo-Carboniferous metasedimentary and Upper Jurassic–Lower Cretaceous volcano-sedimentary strata (Pan et al., 2004), Lower Cretaceous volcanic rocks (e.g., Zenong Group, Zhu et al., 2011), 215–95 Ma plutonic rocks (Zhu et al., 2008), and a small volume of 68–49 Ma granitoids (Zheng et al., 2015). In the southern Lhasa terrane, the most represented geologic units are the Upper Triassic to Paleogene Gangdese magmatic arc (Schärer et al., 1984; Wen et al., 2008; Ji et al., 2009) and the uppermost Cretaceous to Eocene Linzizong volcanic succession (Mo et al., 2008, and references therein), with limited exposures of Upper Triassic-Cretaceous successions (Pan et al., 2006; Zhu et al., 2013). Zircons from the central Lhasa terrane display negative εHf(t) values, suggesting the existence of an ancient crust (Chu et al., 2006; Zhu et al., 2011), whereas positive εHf(t) values characterize zircons from the southern Lhasa terrane, indicating a juvenile crust (Chu et al., 2006; Ji et al., 2009).

South of the Gangdese magmatic arc, the Xigaze forearc basin exposed from Renbu in the east to Zhongba in the west is ~20 km wide (Fig. 1A). The Xigaze forearc-basin succession can be subdivided into a lower underfilled part and an upper overfilled part, with prominent facies and provenance changes recorded ca. 88 Ma (e.g., Wu et al., 2010; Aitchison et al., 2011; An et al., 2014; Orme et al., 2015). The underfilled stage was characterized by deep-water turbidites mainly fed from the Gangdese arc and occasionally from reworking of the Lower Cretaceous carbonates of the Sangzugang Formation. During the subsequent overfilled stage, instead, sedimentation took place in shallower-water to deltaic environments with detritus supplied from the Gangdese arc and the central Lhasa terrane.

The Yarlung-Zangbo ophiolite consists of mantle peridotite, cumulate, gabbro, sheeted dike, pillow lava, and radiolarian chert exposed from Luobusa in the east to Yungbwa in the west. Mafic magmatism was dated initially at 120 ± 10 Ma (Göpel et al., 1984), and then refined by multi-methods as 123–128 Ma (Malpas et al., 2003; Dai et al., 2013 and references therein). Three different models have been proposed to frame its origin: (*i*) slow-spreading mid-ocean ridge (Girardeau et al., 1985a, 1985b), (*ii*) supra-subduction setting (Bédard et al., 2009; Hébert et al., 2012), and (*iii*) forearc spreading (Dai et al., 2013; Huang et al., 2015). The third model is the one best supported by stratigraphic evidence, which conclusively indicates that the ophiolite represents the substratum of the Xigaze forearc basin (An et al., 2014; Wang et al., 2017a).

In tectonic contact with the Yarlung-Zangbo ophiolite to the north and with the Tethyan Himalaya sedimentary zone to the south (Fig. 1B), chaotic units with blocks embedded in siliciclastic matrix have been named variously in the literature (e.g., Xiukang Mélange after XBGMR, 1979; wildflysch with exotic blocks after Tapponnier et al., 1981). These mélange units, traditionally interpreted as representing the Neo-Tethyan subduction system (Tapponnier et al., 1981; Searle et al., 1987; Cai et al., 2012), have been recently documented to have developed at least in part during the initial Paleocene-Eocene stage of the India-Asia collision (An et al., 2017; Metcalf and Kapp, 2017). The Xiukang Mélange is composed of exotic blocks of sandstone, limestone, chert, and basalt set in a deformed matrix of Upper Triassic-Lower Aptian abyssal chert, siliceous mudstone, and locally turbidites (Cai et al., 2012). Sandstone blocks include quartzose petrofacies derived from the Indian passive margin, and Cretaceous to Eocene lithic-rich volcanic petrofacies sourced from the Asian active margin (Cai et al., 2012; Li et al., 2015; An et al., 2017). Abundant and mostly bioclastic-limestone blocks, probably detached from the outer peri-Gondwana shelf or seamounts within the Neo-Tethys Ocean (Shen et al., 2003a, 2003b), yield Middle-Late Permian crinoids and bryozoans, together with foraminifera of Early Triassic, Early Jurassic, and Late Cretaceous age (Tapponnier et al., 1981; Jin et al., 2015, and references therein). Blocks derived from seamounts within the Neo-Tethys Ocean, as recorded by limestone and chert deposited directly on oceanic island basalt (OIB), have been reported in the Zhongba area (Dai et al., 2012). Blocks of radiolarian chert are of two types: A Middle-Upper Triassic group with continental-margin affinity, and an Upper Jurassic–Lower Cretaceous group with oceanic-basin affinity (Zhu et al., 2005).

The Luogangcuo Formation, in tectonic contact with the Xiukang Mélange near Saga and consisting of gray conglomerate, yellow-greenish coarse sandstone and pebbly sandstone, was first described as a Cenozoic unit by Yin et al. (1988) (Fig. 1C). Based on chert clasts with Barremian radiolarian associations and sandstones yielding quartz electron spin resonance (ESR) ages of 41.2–46.2 Ma (Li et al., 2007), the unit was considered as a lower Eocene continental "molasse" comparable to the Liuqu Conglomerate exposed in the Xigaze area.

Bounded along its southern margin by the South Tibet detachment zone, the Tethyan Himalaya represents the remnant of the northern Indian passive margin, separated into northern and southern domains by the Gyirong-Kangmar thrust (Liu and Einsele, 1994; Ratschbacher et al., 1994; Sciunnach and Garzanti, 2012). The southern domain is characterized by Paleozoic to Eocene shelfal carbonates and terrigenous strata (Willems et al., 1996; Jadoul et al., 1998), whereas the northern domain consists of corresponding outer shelf, continental slope, and rise deposits (Liu and Einsele, 1994; Li et al., 2005; Hu et al., 2008).

METHODS

Two stratigraphic sections (Figs. 1C, 2, and 3A), with a total thickness of 200 m, were measured in detail and distinguished into eight lithofacies (Table 1). Thirteen sandstone samples from the Luogangcuo Formation were selected for point-counting according to the Gazzi-Dickinson method (Ingersoll et al., 1984). Over 400 points were counted on each sample. The complete petrographic data set is provided as Data Repository Table DR1[1].

Zircons were separated from eight sandstone samples for U-Pb dating and Hf isotopic analysis. U-Pb dating of the core of detrital grains was performed by laser-ablation–inductively coupled plasma–mass spectrometry (LA-ICP-MS) at the State Key Laboratory of Mineral Deposits Research, Nanjing University, China, using a beam diameter of 35 μm and following the method described by Jackson et al. (2004). The weighted $^{206}Pb/^{238}U$ age of the standard sample Mud Tank Zircon obtained was 740.1 ± 5.0 Ma (n = 53) in agreement with the predicted value (thermal ionization mass spectrometry [TIMS] age 732 ± 5 Ma; Black and Gulson, 1978). Age calculations and relative-age-probability diagrams were created using Isoplot 4.0 (Ludwig, 2011). The interpretation of zircon ages was based on $^{206}Pb/^{238}U$ ages for grains <1000 Ma and on $^{207}Pb/^{206}Pb$ ages for grains >1000 Ma. Ages >200 Ma with discordance >10% and ages <200 Ma with discordance >20% were discarded. The complete data set is provided as Data Repository Table DR2. The maximum depositional age of sedimentary layers was calculated by detrital-zircon chronostratigraphy according to the five methods listed in Table 2. Our preferred method is the weighted mean age of two or more grains overlapping with the

[1]GSA Data Repository Item 2018140, Table DR1: Framework modal analytical results of sandstones from the Luogangcuo Formation; Table DR2: Detrital zircon U-Pb ages from the Luogangcuo Formation; Table DR3: Analyzed detrital zircon Hf isotope data, is available at http://www.geosociety.org/datarepository/2018, or on request from editing@geosociety.org.

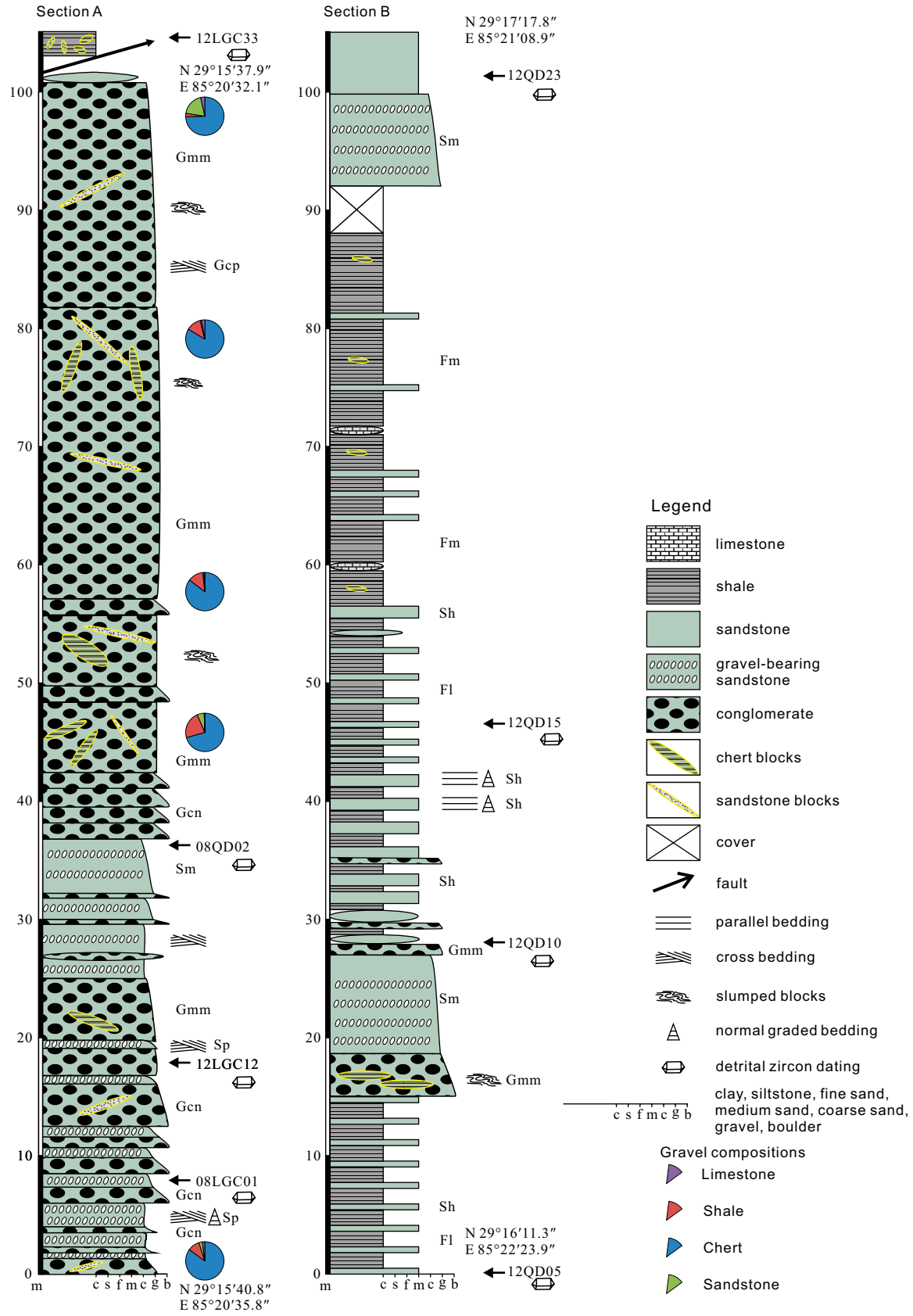

Figure 2. Measured stratigraphic sections of the Luogangcuo Formation. Lithofacies are described in Table 1. Gravel composition and position of samples used for detrital-zircon geochronology are shown.

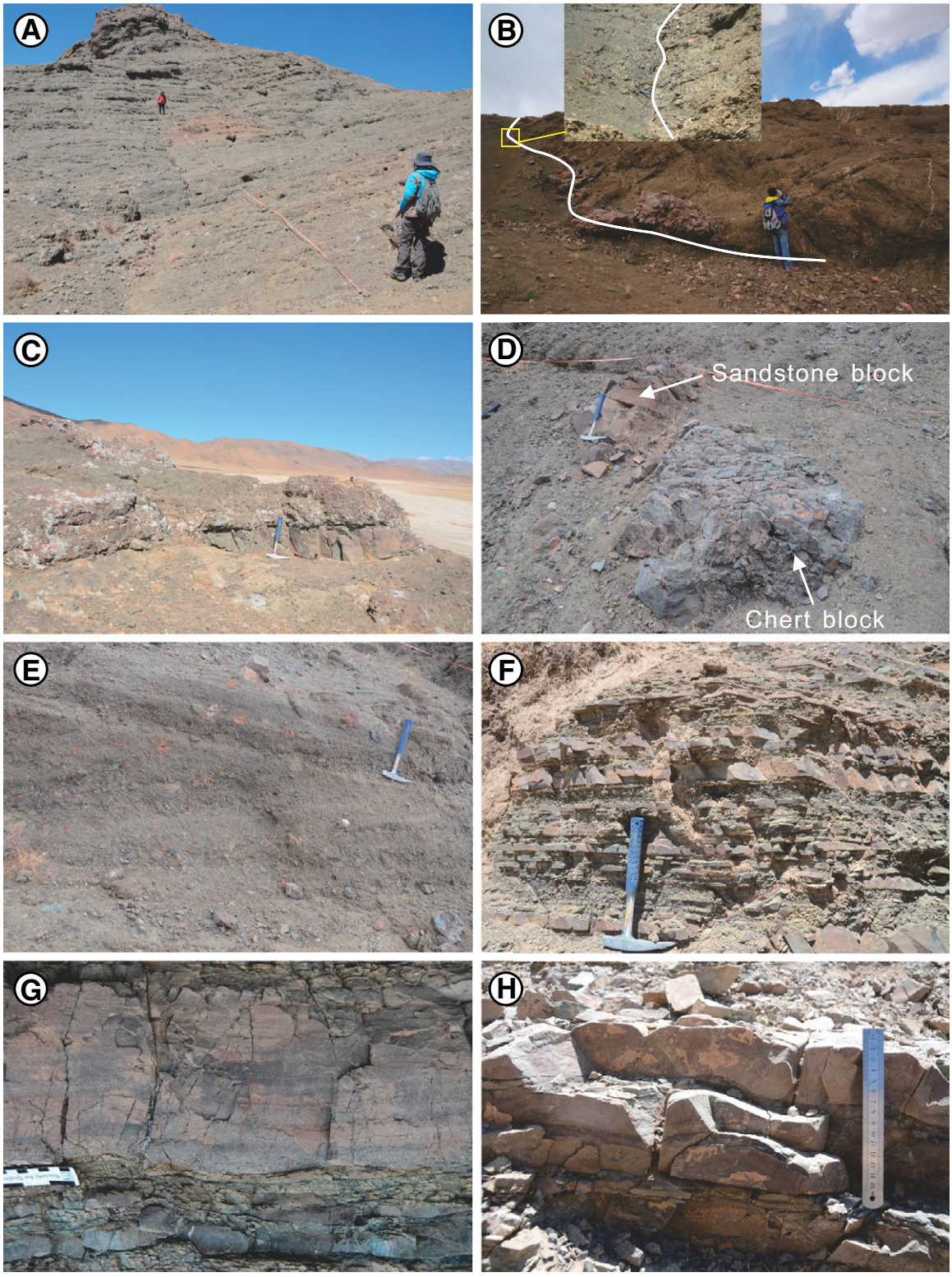

Figure 3. Field photographs of the Luogangcuo Formation. (A) Panorama of Section A. (B) Fault contact between the Xiukang Mélange (left) and the Luogangcuo Formation (right); detail shown in the inset photo. (C) Sandstone lens (Sm) intercalated with matrix-supported conglomerates (Gmm). (D) Slumped blocks of sandstone and chert. (E) Oblique lamination in pebble conglomerates (Gcp). (F) Lithofacies Sh and Fl representing turbiditic layers. (G) Turbiditic sandstone with incomplete Bouma sequence. (H) Thin-bedded sandstones with erosional base.

TABLE 1. LITHOFACIES FOUND IN THE LUOGANGCUO FORMATION, SOUTH TIBET, AND INTERPRETATIONS OF THEIR DEPOSITIONAL PROCEDURE

Facies code	Description	Interpretation
Gcn	Several tens of centimeters to several meters thick, pebble to cobble conglomerate, subround to angular gravel, moderately sorted, clastic-supported, normal grading, beds extend laterally for tens of meters	Clastic-rich debris flow deposits
Gcp	Several tens of centimeters to several meters thick, pebble to cobble conglomerate, subround to angular gravel, moderately sorted, clastic-supported, planar cross-stratified, poorly organized, beds extend laterally for tens of meters	Deposition by large straight-crested gravelly ripples under traction flows in shallow fluvial channels, gravel bars and gravelly Gilbert deltas
Gmm	10-mm- to 1-m-thick, pebble to cobble conglomerate, subround to subangular gravel, poorly sorted, matrix-supported, massive, disorganized, beds extend laterally for tens of meters	Plastic debris flow deposits
Sh	10–30-cm-thick bed, fine- to medium-, normal-grained sandstone with parallel lamination, beds are laterally continuous	Upper plane bed conditions under strong or very shallow unidirectional flows
Sp	10–30-cm-thick bed, fine- to coarse-grained sandstone with planar cross-stratification, pebbly, beds are lensing	Migration of large 2-D ripples under moderately powerful unidirectional channelized flows; migration of sandy transverse bars
Sm	10-mm- to 1-m-thick, massive fine- to coarse-grained sandstone, can be pebbly and have poor normal grading, discontinuous beds	Sand-rich debris flow deposits
Fl	Laminated siltstone or mudstone	Distal fan; suspension fallout
Fm	Massive siltstone or mudstone	Waning gravity flow deposits; suspension fallout

youngest one at 1σ (YC1σ(2+)), which proved to be more consistently compatible with depositional ages of Mesozoic sandstone samples from the Colorado Plateau (Dickinson and Gehrels, 2009).

In situ Hf isotopic analyses were performed on the same spots used for U-Pb age analysis at the State Key Laboratory for Mineral Deposits Research, Nanjing University, with a Thermo Scientific Neptune Plus MC-ICP-MS coupled to a New Wave UP193 solid-state laser-ablation system. We used a beam diameter of 50 μm and an 8-Hz laser repetition rate with energy >15.5 J/cm^2. The Mud Tank standard was analyzed in every run, yielding $^{176}Hf/^{177}Hf = 0.282489 \pm 0.000030$ (2σ; n = 40), which is identical to the literature value of $^{176}Hf/^{177}Hf = 0.282522 \pm 0.000042$ (2σ; n = 2335) (Griffin et al., 2007). The complete data set is provided as Data Repository Table DR3.

SEDIMENTOLOGY OF THE LUOGANGCUO FORMATION

The studied outcrop, in fault contact with the Xiukang Mélange (Fig. 3B), is cut in two by the course of the Yarlung-Zangbo River. Two sections, each ~100 m thick, were measured on either side of the river (Figs. 1C and 2). Owing to poor preservation, the entire thickness of the unit is unknown. Section A, measured south of the Yarlung-Zangbo River, consists of thick-bedded or amalgamated conglomerates with minor thick- to medium-bedded pebble-bearing sandstone intercalated in the lower ~35 m and massive conglomerate in the upper part. Section B, measured to the north, displays more variable lithologies, including rhythmic alternations of thin-bedded sandstone and shale couplets with minor massive conglomerate and pebble-bearing sandstone in the lower part, followed by shale increasing upwards and capped by massive pebble-bearing sandstone. In both sections, blocks of chert, sandstone, and limestone occur in conglomerates or are locally embedded in shale. Eight lithofacies types (Table 1) were distinguished according to Miall (1978) and DeCelles et al. (1991), and grouped into three facies associations according to Mutti and Ricci Lucchi (1978).

Proximal Submarine Fan

Description. This facies association, occurring in Section A (Fig. 3A) and lower part of Section B, comprises predominantly gray-green, moderately to poorly sorted, massive or normal-graded, clast- or matrix-supported conglomerates (lithofacies Gcm, Gcn, Gmm, and Gcp) with angular to subrounded pebbles and cobbles up to 20 cm in diameter. Massive (Sm) (Fig. 3C) or oblique laminated (Sp) pebble-bearing sandstones are scarce. Lithofacies Gcm and Gmm are massive, commonly in sharp contact with exotic blocks of sandstone and chert (up to 1.5 m in diameter; Fig. 3D). Beds of lithofacies Gcn, 0.2–1.5 m thick, include abundant sandy matrix and display normal grading from cobbles at the base to sand at the top. Lithofacies Gcp is thin-bedded, normally graded, and occasionally includes strata with tabular oblique lamination (Fig. 3E). Medium to

TABLE 2. SUMMARIZED CHARACTERISTICS OF DETRITAL ZIRCON U-Pb AGES OF SANDSTONE SAMPLES IN THE LUOGANGCUO FORMATION, SOUTH TIBET

Formation	Sample	Analyzed numbers of zircon grains	Mesozoic ages (%)	YDZ	YSG	YPP	YC1σ(2+)	YC2σ(3+)
Turbidite in section A	08QD02	91	33	79.9 + 1.9/–2.1	80 ± 1	81.2	**81.3 ± 2.9 (n = 3)**	81.3 ± 2.9 (n = 3)
	08LGC01	69	51	79.5 + 1.2/–3	80 ± 1	81.2	**81.2 ± 0.7 (n = 9)**	81.9 ± 0.7 (n = 13)
Turbidite in section B	12QD23	74	62	82.3 + 2.7/–5.2	83 ± 2	87.6	**84.9 ± 1.9 (n = 5)**	87.4 ± 1.2 (n = 12)
	12QD15	64	75	81.8 + 1.9/–2.2	82 ± 1	85.2	**83.0 ± 1.4 (n = 2)**	84.6 ± 1.3 (n = 9)
	12QD10	61	36	85.7 + 2.5/–4.3	86 ± 2	89.0	**88.2 ± 1.8 (n = 5)**	90.1 ± 2.1 (n = 10)
	12QD05	68	35	82.3 + 3.5/–6.1	83 ± 3	86.5	**86.0 ± 2.1 (n = 5)**	88.2 ± 4.1 (n = 7)
Sandstone blocks	12LGC33	63	92	88.3 + 3.1/–7.1	88 ± 3	99.1	**91.9 ± 2 (n = 5)**	94.8 ± 1.0 (n = 17)
	12LGC12	63	89	88.3 + 8.4/–32	94 ± 6	109.5	**102.6 ± 3.9 (n = 7)**	106.5 ± 2.0 (n = 24)

Note: YDZ—age calculated by the "Youngest Detrital Zircon" routine of Isoplot (Ludwig, 2011). YSG—youngest single detrital zircon age with 1σ uncertainty. YPP—youngest graphical detrital zircon age peak on an age-probability plot or age-distribution curve. YC1σ(2+)—weighted mean age (±1σ incorporating both internal analytical error and external systematic error) of youngest cluster of two or more grain ages overlapping with the youngest age at 1σ (Dickinson and Gehrels, 2009). YC2σ(3+)—weighted mean age (±1σ incorporating both internal analytical error and external systematic error) of youngest cluster of three or more grain ages overlapping with the youngest age at 2σ (Dickinson and Gehrels, 2009).

coarse-grained lithofacies Sm and Sp are intercalated within lithofacies Gcn and Gmm, and contain radiolarian chert pebbles. Sandstone beds, ~0.2 m thick, commonly show limited lateral extent and sharp contacts both at the bottom and top. Sedimentary structures are limited to graded-bedding (Gcn) and oblique lamination (Gcp, Sp).

Interpretation. This arenaceous-conglomeratic association was deposited by grain flows or high-concentration turbidity currents in proximal submarine-fan settings (Mutti and Ricci Lucchi, 1978; Underwood and Moore, 1995). Lithofacies Gcm and Gcn suggest channelized high-energy debris flows. Lithofacies Gmm indicates unchannelized debris flows and sudden dumping of the whole sediment load owing to rapid loss of speed. Lithofacies Gcp points to large migrating barforms, which can develop in deep-water conglomeratic fan-feeder systems (Walker, 1975; Satur et al., 2004). Lithofacies Sm and Sp were deposited as channelized turbiditic flows.

Distal Submarine Canyon

Description. Most of Section B is characterized by laminated mudstone (Fl, Fig. 3F), interbedded with normally graded, parallel laminated sandstone (Sh, Figs. 3G and 3H) and massive siliceous mudstone (Fm) with a few slumped blocks of sandstone and chert. Beds of lithofacies Sh, mainly fine or medium-grained and up to 0.6 m thick, commonly display flat base and locally groove casts and Ta-Tb subdivisions of incomplete Bouma sequences (Bouma, 1962). These beds either occur as lenses within lithofacies Fm or pass laterally to lithofacies Fl intercalations.

Interpretation. This arenaceous association was deposited on a distal submarine fan or deep-sea plain by turbidity currents and diluted low-density turbidity currents with suspension fallout (Mutti and Ricci Lucchi, 1978; Underwood and Moore, 1995). Finer-grained than sediments in the proximal submarine fan, lithofacies Sh was deposited from the low-concentration tail of higher-density turbidity currents (e.g., Mutti, 1992; DeCelles et al., 2014). Lithofacies Fm and Fl represent background sedimentation dominated by suspension fallout.

Submarine Olistoliths

Description. Allochthonous blocks of sandstone and chert up to 1.5 m in diameter (Fig. 3D) occur in both sections, mostly within massive conglomerates (lithofacies Gcm and Gmm) and occasionally embedded in massive mudstones (Fm). Sharp contacts, disrupted stratification, and deformation around the blocks are commonly observed.

Interpretation. This chaotic facies originated by large-scale submarine slumps on a slope triggering debris flows or mud flows (Mutti and Ricci Lucchi, 1978; Underwood and Moore, 1995). Similar deposits are widely reported in turbidite sequences, from the northern Apennines (Mutti and Ricci Lucchi, 1978) to the Yarlung-Zangbo suture zone (Wang et al., 2011; DeCelles et al., 2014).

PROVENANCE ANALYSIS

Conglomerate and Sandstone Petrography

The Luogangcuo conglomerates are polymictic, with poorly sorted, angular to subrounded clasts set in a sandy matrix. In Section A, granules to cobbles consist of radiolarian chert (70%–85%, Fig. 4A), subordinate shale (3%–23%), sandstone (1%–20%), and minor limestone (<4%) (Fig. 2; Fig. 4B). Clast size is finer in Section B, with similarly dominant chert.

The turbiditic sandstones are feldspatho-quartzo-lithic volcaniclastic, with average modal composition quartz:feldspar:lithic (Q:F:L) = 33:21:46 in Section A and Q:F:L = 27:24:49 in Section B (Fig. 5A). Mostly monocrystalline quartz grains are angular to subrounded and show uniform extinction (Figs. 4C–4F). Plagioclase is much more abundant than K-feldspar (Fig. 4D). Lithic fragments, representing 35%–63% of framework grains (Fig. 5B), are mainly andesite and rhyolite. Subordinate sedimentary (shale, siltstone, chert) and minor low-rank metamorphic lithics (slate) also occur.

Sandstone blocks are quartzo-feldspatho-lithic volcaniclastic (Fig. 4G), with average composition Q:F:L = 10:31:59 (Fig. 5A). Lithic fragments, representing 45%–73% of framework grains (Fig. 5B), are mainly basalt and andesite. Sedimentary lithics (limestone, siltstone, chert) are subordinate. Metamorphic rock fragments were not observed. Chert blocks and pebbles in conglomerates contain abundant radiolarians (Fig. 4H).

Detrital Zircon Geochronology and Hf Isotopes

Two turbiditic sandstones in Section A (08QD02 and 08LGC01) yielded 65 zircon grains with Mesozoic U-Pb age and another 95 grains of older ages (Fig. 6A). The ages of the three youngest grains are 80 ± 1 Ma, 80 ± 1 Ma, and 81 ± 1 Ma (discordance 1.2%, 6.2%, and –4.9%, respectively). The YC1σ(2+) ages of the two samples are 81.3 ± 2.9 and 81.9 ± 0.7 Ma. Age spectra exhibit a prominent young cluster between 80 and 146 Ma with main peak at 81.2 Ma, and a subordinate cluster between 450 and 600 Ma with main peak at 548 Ma. Sixty zircon grains with Mesozoic age yielded εHf(t) values ranging widely from –25.7 to +13.5 (Fig. 6F).

Four turbiditic sandstones in Section B (12QD05, 12QD 10, 12QD 15, and 12QD 23) yielded 141 zircon grains with Mesozoic age and 126 grains with older ages (Fig. 6B). The ages of the three youngest grains are 82 ± 1 Ma, 83 ± 1 Ma, and 93 ± 3 Ma (discordance 0%, 0%, and 1.1%, respectively). The YC1σ(2+) ages of the four samples are 86.0 ± 2.1, 88.2 ± 1.8 Ma, 83.0 ± 1.4 Ma, and 84.9 ± 1.9 Ma, respectively. Age spectra are complex, with a young cluster between 86 and 146 Ma with main peak at 88 Ma. Seventy-three grains with Mesozoic age yielded εHf(t) values ranging widely from –13.0 to +17.3 (Fig. 6G).

Two sandstone blocks (12LGC12 and 12LGC33) yielded 114 zircon grains with Mesozoic age and 12 grains with older ages (Fig. 6C). The ages of the three youngest grains are 88 ± 3 Ma, 91 ± 3 Ma, and 92 ± 2 Ma (all 0% discordance). The YC1σ(2+) ages of the two samples are 91.9 ± 2 Ma and 102.6 ± 3.9 Ma. Age spectra display a single cluster between 91 and 211 Ma, with main peak at 102 Ma. Seventy-eight Mesozoic grains yielded mostly positive εHf(t) values up to +14.7, and only three negative values down to –13.7 (Fig. 6H).

Provenance Interpretation

A different magmatic evolution characterized the central and southern Lhasa terranes. Zircons from magmatic rocks of the central Lhasa terrane yield ages mostly in the 230–180 Ma and 140–100 Ma range (peak at ca. 110 Ma) and negative εHf(t) values (Zhu et al., 2011, and references therein). Zircons from magmatic rocks of the southern Lhasa terrane, emplaced between the Late Triassic and the Eocene (220–40 Ma), display instead positive εHf(t) values (Chu et al., 2006; Ji et al., 2009). In stark contrast, detrital zircons derived from the northern Indian subcontinent are mostly characterized by Proterozoic to early Paleozoic ages (DeCelles et al., 2004; Zhu et al., 2011), with an Early Cretaceous (140–119 Ma, peak at 138 Ma) cluster characterized by negative εHf(t) values (Hu et al., 2010; Wu et al., 2014). Additionally, andesitic-rhyolitic volcanic detritus shed from the central and southern Lhasa terranes contrasts with quartzose detritus locally containing basaltic rock fragments derived from northern India (Hu et al., 2010, 2015).

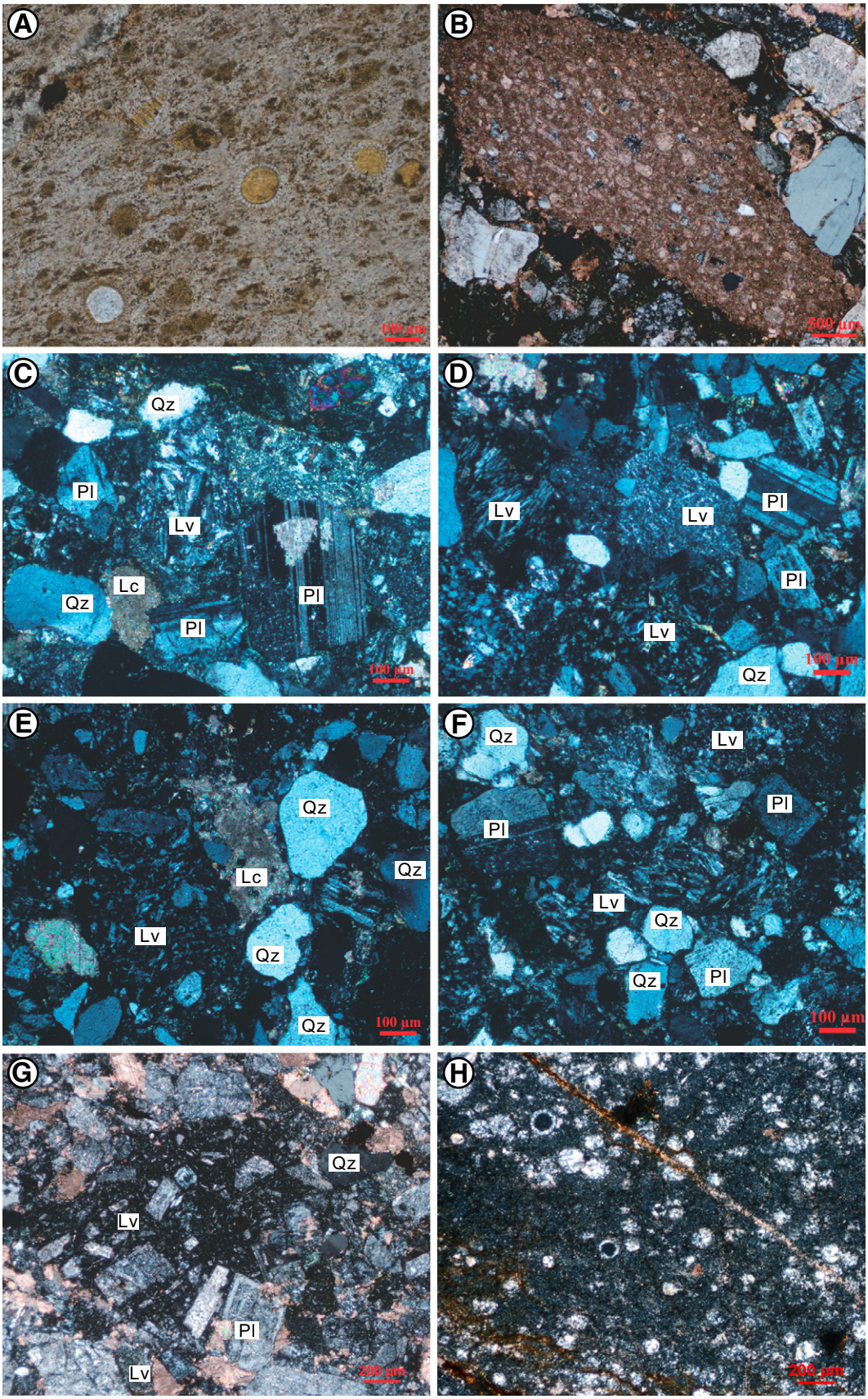

Figure 4. Petrofacies of the Luogangcuo Formation: (A) Radiolarian chert. (B) Impure bioclastic-limestone clasts in conglomerates (samples 12QD02 and 12LGC12). (C–F) Quartzo-feldspatho-lithic volcaniclastic sandstones (12LGC05, 12QD04, 12QD17, and 12QD20). (G–H) Slumped blocks of feldspatho-lithic volcaniclastic sandstone and radiolarian chert (12LGC15 and 12LGC19). Qz—quartz; Pl—plagioclase; Lv—volcanic lithic; Lc—carbonate lithic.

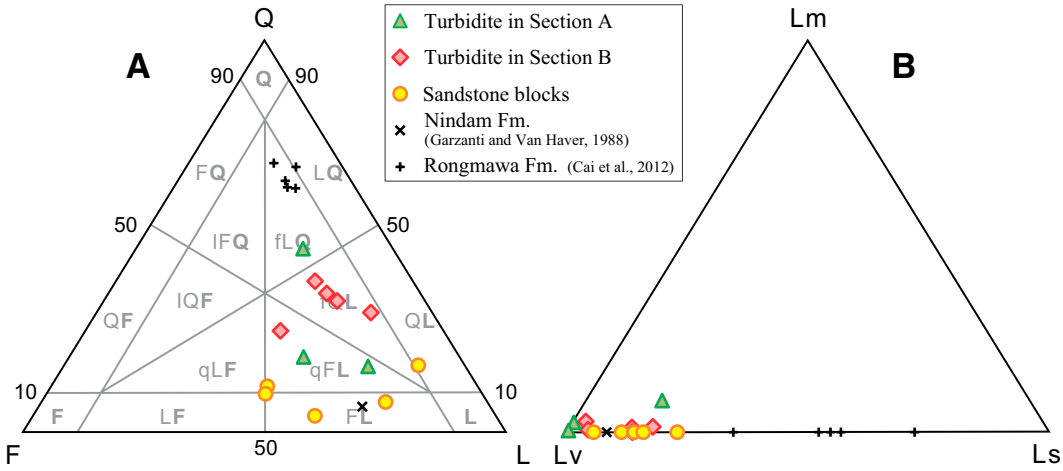

Figure 5. Ternary diagrams showing the petrographic composition of turbiditic sandstones and sandstone blocks in the Luogangcuo Formation. (A) QFL diagram, petrographic classification after Garzanti (2016). (B) LmLvLs diagram. Q—quartz; F—feldspar; L—lithic fragments (Lm—metamorphic; Lv—volcanic; Ls—sedimentary). Data for the Nindam Formation and mélange from Garzanti and Van Haver (1988) and for the Rongmawa Formation from Cai et al. (2012).

In the Xigaze forearc basin, the middle-lower Ngamring Formation contains detrital zircons with typical Gangdese arc signatures (Mesozoic ages and positive εHf(t) values), whereas the upper Ngamring and Padana formations yield numerous zircon grains with either pre-Mesozoic or Mesozoic ages and positive or negative εHf(t) values, testifying to provenance from both Gangdese arc and central Lhasa terrane (Wu et al., 2010; An et al., 2014; Orme et al., 2015; Orme and Laskowski, 2016). Adjacent to the Luogangcuo Formation, the Xiukang Mélange contains numerous blocks of: (*i*) Upper Cretaceous to Eocene lithic-rich volcaniclastic sandstones derived from the Gangdese arc and central Lhasa terrane, (*ii*) pre-Cretaceous quartzose sandstones derived from the Indian subcontinent; and, (*iii*) Middle Triassic to Lower Cretaceous chert or Middle Permian to Upper Cretaceous limestone derived either from the distal Indian margin or the Neo-Tethyan oceanic domain (Shen et al., 2003a, 2003b; Cai et al., 2012; An et al., 2017; Metcalf and Kapp, 2017).

Among all of the potential sediment sources described above, recycling of the Xiukang Mélange exposed nearby is the most probable one for the Luogangcuo conglomerates, the textural features of which indicate limited transport driven by gravity. The same radiolarian assemblages of Barremian age (129–125 Ma) found in the abundant chert clasts within the Luogangcuo Formation have been reported from chert blocks of the Xiukang Mélange in the Saga area (Li et al., 2007), interpreted as deposited originally on Neo-Tethyan Ocean crust and subsequently accreted tectonically in the subduction complex. Detritus in the Luogangcuo sandstones is dominated by andesitic and rhyolitic volcanic rock fragments, and detrital zircons yield pre-Mesozoic and Mesozoic ages with both positive and negative εHf(t) values, suggesting provenance directly from the Gangdese arc and central Lhasa terrane. Modal composition and zircon-age patterns in Luogangcuo sandstones compare well with the detrital signatures of both upper Ngamring and Padana sandstones of the Xigaze forearc basin (Wu et al., 2010; Aitchison et al., 2011; An et al., 2014; Orme et al., 2015) and Cretaceous lithic-rich volcaniclastic sandstone blocks of the Xiukang Mélange (Cai et al., 2012; Li G.W. et al., 2015; An et al., 2017). The modal composition of the Luogangcuo sandstones resembles that of the Nindam Formation in the Ladakh Himalaya, India (Garzanti and Van Haver, 1988), but includes more volcanic rock fragments compared to the Rongmawa Formation in the Ngamring area, south Tibet (Cai et al., 2012), suggesting supply mostly from the Gangdese arc. The studied sandstone olistoliths display volcaniclastic composition and predominant Mesozoic zircons with positive εHf(t) values, comparing well with detrital modes and zircon-age patterns of lower Ngamring sandstones derived from the Gangdese arc (Wu et al., 2010; Aitchison et al., 2011; An et al., 2014; Orme et al., 2015). All of the observed sedimentologic, petrographic, geochronologic and geochemical features concur to indicate that the Luogangcuo conglomerates and slumped blocks were eroded from the Xiukang Mélange and/or recycled from the Xigaze forearc basin, whereas turbiditic sandstones may have been derived directly from the Gangdese arc and central Lhasa terrane.

DISCUSSION

Depositional Age

Because the Luogangcuo Formation lacks fossils and interbedded tuffs, its depositional age could not be constrained robustly so far. A depositional age of ca. 41.2–46.2 Ma was inferred by quartz electron spin resonance dating (Li et al., 2007), a technique usually performed on Quaternary sediments (Burdette et al., 2013; Duval et al., 2015) and the accuracy of which is generally considered as limited to the Pliocene (Laurent et al., 1998; Rink et al., 2007). Detrital-zircon chronostratigraphy represents a much more reliable approach for dating volcaniclastic sediments deposited within an arc-trench system including a magmatic arc, because they are likely to contain zircon grains as young, or almost as young as their depositional age (Amato and Pavlis, 2010; Kochelek et al., 2011; Orme et al., 2015). Five different chronostratigraphic methods to define the most likely depositional age were tested by Dickinson and Gehrels (2009). Ranked from the least to the most statistically robust, they are: YDZ, YSG, YPP, YC1σ(2+), and YC2σ(3+) (see Table 2 for explanation). The youngest detrital-zircon age YDZ calculated from Isoplot represents a poor criterion, because it is prone to underestimate depositional age and is therefore not recommended. On the other hand, YC2σ(3+) is prone to overestimate depositional age (fig. 8 and table 2 in Dickinson and Gehrels, 2009). YC1σ(2+) is thus the method preferred here. All the five methods are illustrated in Table 2, which shows that YSG, YPP, and YC1σ(2+) ages are all similar, whereas the YDZ age is younger and the YC2σ(3+) age slightly older.

Sandstones and conglomerates of the Luogangcuo Formation, largely consisting of detritus shed from Mesozoic to Cenozoic igneous rocks, are undoubtedly deposited as part of the Gangdese arc-trench system. The YC1σ(2+) ages of Luogangcuo sandstones are comprised in a narrow range: 88–83 Ma in Section B, and 81–82 Ma in Section A. The YC1σ(2+) ages of sandstone olistoliths in Section A range between 103 and 91 Ma, and chert blocks and pebbles yielded Barremian radiolaria (Li et al., 2007). These data suggest that sandstones of the Luogangcuo

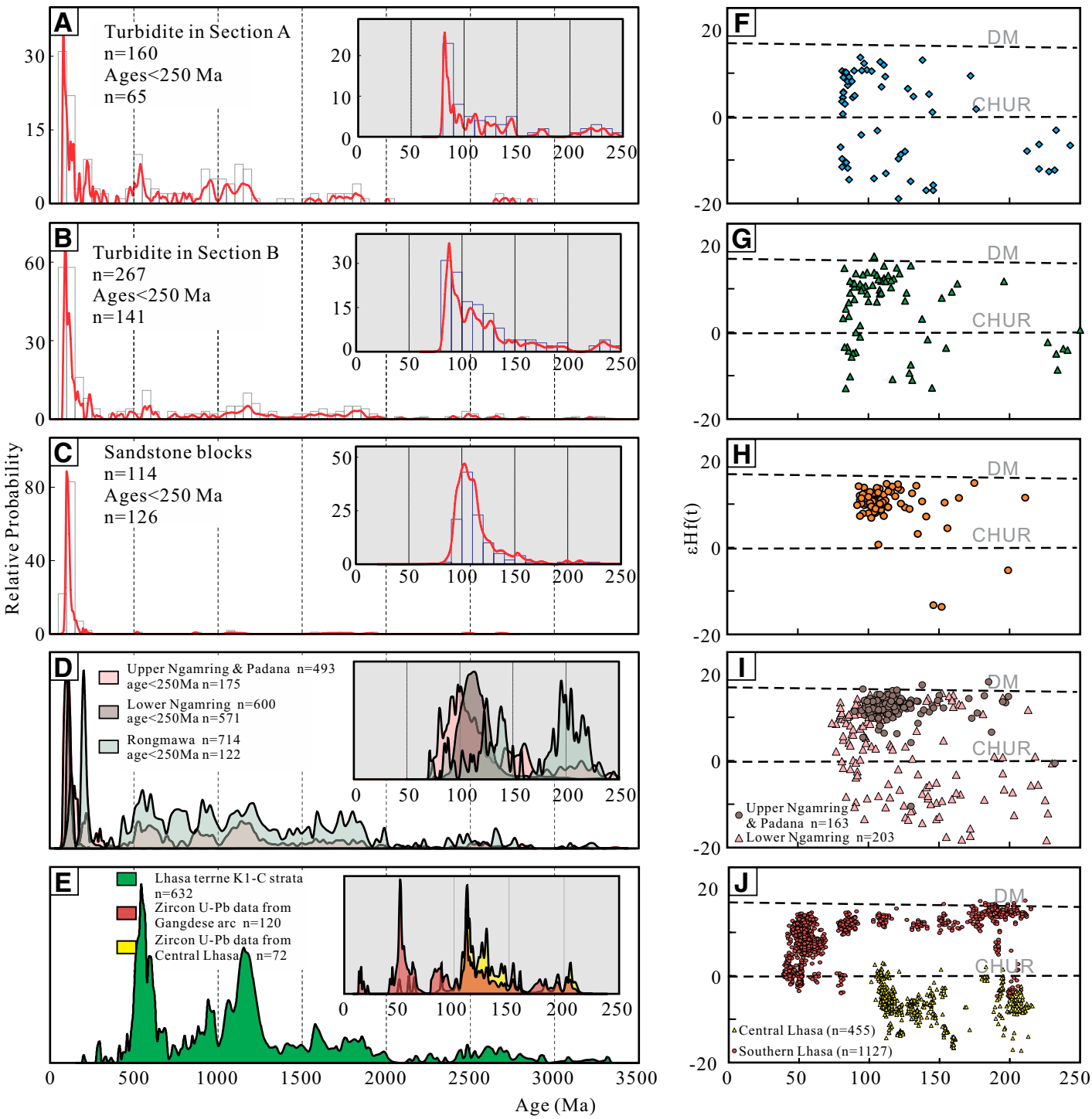

Figure 6. Age patterns (A–C) and Hf isotope signatures (F–H) of detrital zircons in sandstones and slump blocks of the Luogangcuo Formation. Shown for comparison are data from the Xigaze forearc basin (D, I; Wu et al., 2010; Aitchison et al., 2011; An et al., 2014; Orme et al., 2015), Rongmawa Formation (Cai et al., 2012), Gangdese magmatic arc (E, J; Zhu et al., 2008; Wen et al., 2008; Ji et al., 2009, and references therein), and central Lhasa magmatic rocks (Zhu et al., 2011 and references therein) and Carboniferous–Lower Cretaceous strata (Leier et al., 2007; Gehrels et al., 2011; Zhu et al., 2011). DM—depleted mantle; CHUR—chondritic uniform reservoir.

Formation were deposited at Coniacian to early Campanian times (88–81 Ma), and contained blocks of recycled mid-Cretaceous sandstones and Lower Cretaceous cherts. The lack of zircon grains <80 Ma rules out a Cenozoic depositional age, because volcanism has continued well into the Eocene. A source for younger zircon grains has existed through the early Paleogene, as documented in the Paleocene Sangdanlin and Zheya formations nearby (Wang et al., 2011; DeCelles et al., 2014; Wu et al., 2014; Hu et al., 2015, 2017), and not only as ash fall but even in the case of exclusive recycling of the Xiukang Mélange (An et al., 2017).

Depositional Setting

Section A represents proximal submarine-fan deposits dominated by conglomerates with olistoliths and interbedded turbiditic sandstones, whereas Section B consists of more distal turbidites, subordinate conglomerates and slumped blocks. Dominance of chert clasts, derived from chert blocks embedded in the subduction complex, points to an intra-oceanic trench or trench-slope setting. Predominant volcanic rock fragments and lack of clasts recycled from the Xiukang Mélange suggest that turbiditic sandstones were derived directly from the southern Asian margin. Detritus was conveyed through submarine canyons cutting across the subduction complex and connecting the forearc-basin shelf with the trench, an envisaged paleogeographic scenario similar to the modern trench-slope offshore Washington and Oregon (Underwood and Moore, 1995, their fig. 5.10). Zircon chronostratigraphy indicates that strata exposed in the more distal Section B may be slightly older than the proximal submarine-fan deposits of Section A, documenting in this case an upward-coarsening succession typical of trench deposits (Lash, 1985; Underwood and Moore, 1995). Similar sedimentary units have been recognized in several subduction systems worldwide and interpreted as trench fill. One example is the Upper Cretaceous McHugh Creek assemblage exposed seaward of the Chugach–Prince William accretionary prism in Alaska, USA, which includes turbiditic sandstones and conglomerates sourced mainly from the adjacent magmatic arc and subordinately from the forearc basin and subduction complex (Nilsen and Zuffa, 1982; Kochelek et al., 2011; Amato et al., 2013).

In alternative, a trench-slope-basin setting may be envisaged for the Luogangcuo Formation. Previous studies, however, have suggested that the Transhimalayan subduction complex was rather small without large ridges or thrust slices before the onset of the initial India-Asia collision (An et al., 2017; Metcalf and Kapp, 2017), and therefore insufficiently wide and prominent to host a trench-slope basin on top. Most important, the Luogangcuo Formation lies in fault contact with the Xiukang Mélange. A depositional contact with the underlying subduction complex, as displayed for instance by the Cambria, Pfeiffer Beach, and Point San Luis trench-slope basins atop the Franciscan complex, California, USA (Smith et al., 1979), is exposed nowhere. If the Luogangcuo Formation were deposited on top of the subduction complex, then subsequent strong deformation would be required to totally obscure the original depositional contact, which we do not observe. The Luogangcuo Formation is thus interpreted to document sediments deposited in the Neo-Tethyan trench during the Late Cretaceous (Fig. 7).

Sediment Dispersal

Remnants of sedimentary basins within the Transhimalayan arc-trench system include the Xigaze forearc-basin succession, dismembered trench-slope deposits preserved as Cretaceous sandstone blocks within the Xiukang Mélange, and trench or trench-slope deposits including the Luogangcuo Formation described here. After the onset of Neo-Tethyan subduction in the Early Cretaceous, abyssal sediments and seamounts were offscraped and accreted episodically to form a small subduction complex (Dupuis et al., 2005, 2006; Cai et al., 2012; An et al., 2017). Radiolarian cherts of Late Barremian to Aptian age (ca. 126–113 Ma) were deposited on top of the ophiolitic forearc crust (Chongdui Formation; Wang et al., 2017a), overlain in turn by deep-water turbidites fed from the Gangdese arc and accommodated in the underfilled Xigaze forearc basin since ca. 113 Ma (lower-middle Ngamring Formation; Wu et al., 2010; Wang et al., 2012; An et al., 2014; Orme and Laskowski, 2016; Wang et al., 2017b). Since the Coniacian (ca. 88 Ma), abundant igneous detritus shed from both the Gangdese arc and the central Lhasa terrane filled up rapidly the Xigaze forearc basin, as documented by its shallowing-upward, slope-to-shelf-to-deltaic succession (upper Ngamring and Padana formations; Wu et al., 2010; Wang et al., 2012; An et al., 2014; Orme et al., 2015). During this stage, igneous detritus from the Lhasa block started to overspill the forearc basin and reach via submarine canyons the trench and/or trench-slope basins, where distal turbidites were overlain by conglomerates including olistoliths slumped downslope from the subduction complex.

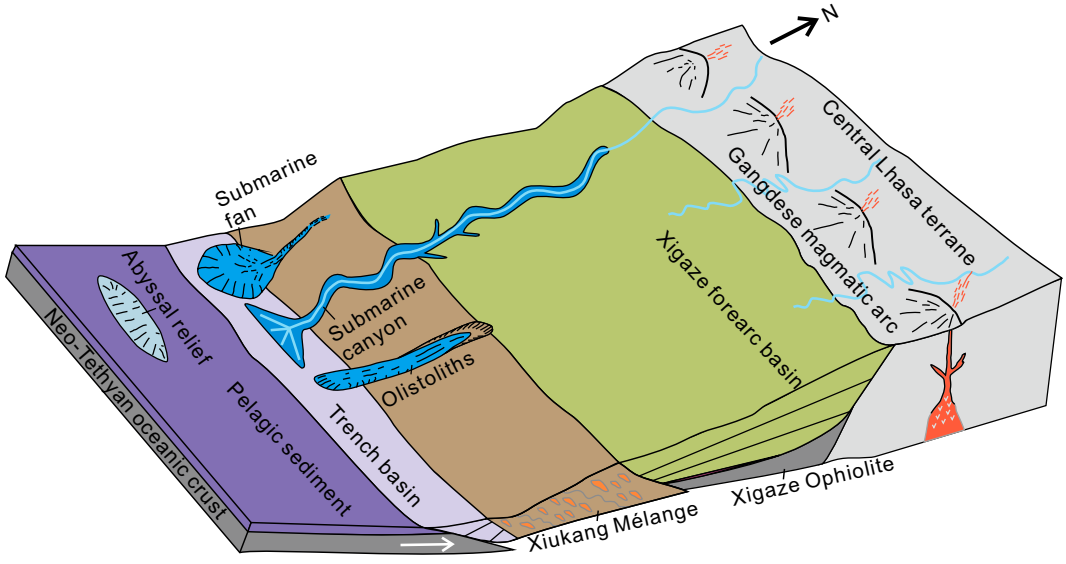

Figure 7. Paleogeographic reconstruction (not to scale), showing the Neo-Tethyan oceanic trench where the Luogangcuo Formation was deposited.

Uplift of the central Lhasa terrane, widening of the source area, and increased sediment volumes at ca. 88 Ma were thus the concomitant factors controlling deposition of the Luogangcuo Formation. A similar evolution is recorded by the western North America arc-trench system, where Jurassic to Neogene successions were deposited progressively in a series of discontinuous forearc basins sourced mainly from the Sierra Nevada and adjacent highlands in the east (e.g., DeGraaff-Surpless et al., 2002; Sharman et al., 2015). During the middle Eocene, source areas expanded toward the continental interior to include also the Idaho Batholith, and detritus bypassed the forearc basin to fill the trench, now included in the Costal Belt subunit of the Franciscan Complex (Dumitru et al., 2013; Sharman et al., 2015).

Transhimalayan trench-fill and trench-slope deposits, also documented in the western Himalaya (Nindam Formation and mélange unit of Garzanti and Van Haver, 1988), were dismembered during subsequent subduction stages and/or early collisional evolution, and are now preserved only as randomly oriented blocks in the Xiukang Mélange (An et al., 2017) or in small local outcrops as the Rongmawa Formation in the Ngamring area (Cai et al., 2012) and the Luogangcuo Formation documented here.

CONCLUSIONS

The Luogangcuo Formation, interpreted to represent trench-fill deposits in the Neo-Tethyan subduction system, provide additional information to unravel patterns of sediment dispersal and the erosional history of the southern Asian margin in the Late Cretaceous. Stratigraphic, sedimentologic, and provenance analyses led us to the following conclusions.

(1) The Luogangcuo Formation, including conglomerates, sandstones, and olistoliths, consists of deep-sea fan turbidites deposited in the Neo-Tethyan trench during the Late Cretaceous (88–81 Ma).

(2) Conglomerate clasts are mostly radiolarian chert, with subordinate lithic-rich volcaniclastic sandstones, siltstones, and limestones recycled from the adjacent Xiukang Mélange. Turbiditic sandstones may have been derived directly from the Lhasa block on the Asian active margin.

(3) Detritus from the Gangdese magmatic arc was initially deposited in the underfilled Xigaze forearc basin since ca. 113 Ma (lower-middle Ngamring Formation). Since ca. 88 Ma, enhanced detrital volumes shed also from the actively uplifting central Lhasa terrane filled the forearc (upper Ngamring-Padana formations), were funneled in submarine canyons cutting across the trench-slope break, and eventually deposited along the trench.

ACKNOWLEDGMENTS

This work benefited from careful critical suggestions by editor Laurent Godin, reviewers Devon Orme and anonymous, and discussion with Jiangang Wang. We thank Bin Wu, Xiong Yan for assistance in the laboratory, and Juan Li, Hanpu Fu for assistance in the field. This study was supported financially by the National Natural Science Foundation of China, NSFC Projects (41525007, 41602115).

REFERENCES CITED

Aitchison, J.C., Xia, X., Baxter, A.T., and Ali, J.R., 2011, Detrital zircon U–Pb ages along the Yarlung-Tsangpo suture zone, Tibet: Implications for oblique convergence and collision between India and Asia: Gondwana Research, v. 20, no. 4, p. 691–709, https://doi.org/10.1016/j.gr.2011.04.002.

Allégre, C.J., Courtillot, V., Tapponnier, P., Hirn, A., Mattauer, M., Coulon, C., Jaeger, J.J., Achache, J., Scharer, U., Marcoux, J., Burg, J.P., Girardeau, J., Armijo, R., Gariepy, C., Gopel, C., Li, T., Xiao, X., Chang, C., Li, G., Lin, B., Teng, J., Wang, N., Chen, G., Han, T., Wang, X., Den, W., Sheng, H., Cao, Y., Zhou, J., Qiu, H., Bao, P., Wang, S., Wang, B., Zhou, Y., and Xu, R., 1984, Structure and evolution of the Himalaya-Tibet orogenic belt: Nature, v. 307, no. 5946, p. 17–22, https://doi.org/10.1038/307017a0.

Amato, J.M., and Pavlis, T.L., 2010, Detrital zircon ages from the Chugach terrane, southern Alaska, reveal multiple episodes of accretion and erosion in a subduction complex: Geology, v. 38, no. 5, p. 459–462, https://doi.org/10.1130/G30719.1.

Amato, J.M., Pavlis, T.L., Clift, P.D., Kochelek, E.J., Hecker, J.P., Worthman, C.M., and Day, E.M., 2013, Architecture of the Chugach accretionary complex as revealed by detrital zircon ages and lithologic variations: Evidence for Mesozoic subduction erosion in south-central Alaska: Geological Society of America Bulletin, v. 125, no. 11–12, p. 1891–1911, https://doi.org/10.1130/B30818.1.

An, W., Hu, X., Garzanti, E., BouDagher-Fadel, M.K., Wang, J., and Sun, G., 2014, Xigaze forearc basin revisited (South Tibet): Provenance changes and origin of the Xigaze Ophiolite: Geological Society of America Bulletin, v. 126, no. 11–12, p. 1595–1613, https://doi.org/10.1130/B31020.1.

An, W., Hu, X., and Garzanti, E., 2017, Sandstone provenance and tectonic evolution of the Xiukang Mélange from Neotethyan subduction to India–Asia collision (Yarlung-Zangbo suture, south Tibet): Gondwana Research, v. 41, p. 222–234, https://doi.org/10.1016/j.gr.2015.08.010.

Armstrong, R., 1991, The persistent myth of crustal growth: Australian Journal of Earth Sciences, v. 38, no. 5, p. 613–630, https://doi.org/10.1080/08120099108727995.

Bédard, É., Hébert, R., Guillemot, C., Le sage, G., Wang, C.S., and Postal, J., 2009, Petrology and geochemistry of the Saga and Sangsang ophiolitic massifs, Yarlung Zangbo Suture Zone, Southern Tibet: Evidence for an arc–back-arc origin: Lithos, v. 113, no. 1–2, p. 48–67, https://doi.org/10.1016/j.lithos.2009.01.011.

Black, L., and Gulson, B., 1978, The age of the mud tank carbonatite, Strangways Range, Northern Territory: BMR Journal of Australian Geology and Geophysics, v. 3, no. 3, p. 227–232.

Bouma, A., 1962, Sedimentology of Some Flysch Deposits: A Graphic Approach to Facies Interpretation: Amsterdam, Netherlands, Elsevier, 168 p.

Burdette, K.E., Rink, W.J., Mallinson, D.J., Means, G.H., and Parham, P.R., 2013, Electron spin resonance optical dating of marine, estuarine, and aeolian sediments in Florida, USA: Quaternary Research, v. 79, no. 1, p. 66–74, https://doi.org/10.1016/j.yqres.2012.10.001.

Busby, C.J., and Ingersoll, R.V., editors, 1995, Tectonics of Sedimentary Basins: Cambridge, Massachusetts, USA, Blackwell Science, 579 p.

Cai, F., Ding, L., Leary, R.J., Wang, H., Xu, Q., Zhang, L., and Yue, Y., 2012, Tectonostratigraphy and provenance of an accretionary complex within the Yarlung–Zangpo suture zone, southern Tibet: Insights into subduction–accretion processes in the Neo-Tethys: Tectonophysics, v. 574–575, p. 181–192, https://doi.org/10.1016/j.tecto.2012.08.016.

Chu, M., Chung, S., Song, B., Liu, D., O'Reilly, S.Y., Pearson, N.J., Ji, J., and Wen, D., 2006, Zircon U-Pb and Hf isotope constraints on the Mesozoic tectonics and crustal evolution of southern Tibet: Geology, v. 34, no. 9, p. 745–748, https://doi.org/10.1130/G22725.1.

Dai, J., Wang, C., and Li, Y., 2012, Relicts of the Early Cretaceous seamounts in the central-western Yarlung-Zangbo Suture Zone, southern Tibet: Journal of Asian Earth Sciences, v. 53, p. 25–37, https://doi.org/10.1016/j.jseaes.2011.12.024.

Dai, J., Wang, C., Polat, A., Santosh, M., Li, Y., and Ge, Y., 2013, Rapid forearc spreading between 130 and 120 Ma: Evidence from geochronology and geochemistry of the Xigaze ophiolite, southern Tibet: Lithosphere, v. 172–173, p. 1–16, https://doi.org/10.1016/j.lithos.2013.03.011.

DeCelles, P., Graym, B., Ridgway, K., Coler, B., Srivastav, P., Pequera, N., and Pivnik, D., 1991, Kinematic history of foreland uplift determined from Paleocene synorogenic conglomerate, Beartooth Range, Wyoming and Montana: Geological Society of America Bulletin, v. 103, p. 1458–1475, https://doi.org/10.1130/0016-7606(1991)103<1458:KHOAFU>2.3.CO;2.

DeCelles, P., Gehrels, G., Najman, Y., Martin, A., Carter, A., and Garzanti, E., 2004, Detrital geochronology and geochemistry of Cretaceous–Early Miocene strata of Nepal: Implications for timing and diachroneity of initial Himalayan orogenesis: Earth and Planetary Science Letters, v. 227, no. 3, p. 313–330, https://doi.org/10.1016/j.epsl.2004.08.019.

DeCelles, P., Kapp, P., Gehrels, G., and Ding, L., 2014, Paleocene-Eocene foreland basin evolution in the Himalaya of southern Tibet and Nepal: Implications for the age of initial India-Asia collision: Tectonics, v. 33, no. 5, p. 824–849, https://doi.org/10.1002/2014TC003522.

DeGraaff-Surpless, K., Graham, S.A., Wooden, J.L., and McWilliams, M.O., 2002, Detrital zircon provenance analysis of the Great Valley Group, California: Evolution of an arc-forearc system: Geological Society of America Bulletin, v. 114, no. 12, p. 1564–1580, https://doi.org/10.1130/0016-7606(2002)114<1564:DZPAOT>2.0.CO;2.

Dewey, J.F., Shackleton, R.M., Chang, C., and Sun, Y., 1988, The tectonic evolution of the Tibetan Plateau: Philosophical Transactions of the Royal Society of London Series A, Mathematical, Physical and Engineering Sciences, v. 327, no. 1594, p. 379–413, https://doi.org/10.1098/rsta.1988.0135.

Dickinson, W.R., 1995, Forearc basins, *in* Busby, C.J., and Ingersoll, R.V., eds., Tectonics of Sedimentary Basins: Cambridge, Massachusetts, USA, Blackwell Science, p. 211–261.

Dickinson, W.R., and Gehrels, G.E., 2009, Use of U–Pb ages of detrital zircons to infer maximum depositional ages of strata: A test against a Colorado Plateau Mesozoic database: Earth and Planetary Science Letters, v. 288, no. 1, p. 115–125, https://doi.org/10.1016/j.epsl.2009.09.013.

Dumitru, T.A., Ernst, W.G., Wright, J.E., Wooden, J.L., Wells, R.E., Farmer, L.P., Kent, A.J.R., and Graham, S.A., 2013, Eocene extension in Idaho generated massive sediment floods into the Franciscan trench and into the Tyee, Great Valley, and Green River basins: Geology, v. 41, no. 2, p. 187–190, https://doi.org/10.1130/G33746.1.

Dupuis, C., Hébert, R., Dubois-Côté, V., Guilmette, C., Wang, C.S., Li, Y.L., and Li, Z.J., 2005, The Yarlung-Zangbo Suture Zone ophiolitic mélange (southern Tibet): New insights from geochemistry of ultramafic rocks: Journal of Asian Earth Sciences, v. 25, no. 6, p. 937–960, https://doi.org/10.1016/j.jseaes.2004.09.004.

Dupuis, C., Hébert, R., Dubois-Côté, V., Guilmette, C., Wang, C.S., and Li, Z.J., 2006, Geochemistry of sedimentary rocks from mélange and flysch units south of the Yarlung-Zangbo suture zone, southern Tibet: Journal of Asian Earth Sciences, v. 26, no. 5, p. 489–508, https://doi.org/10.1016/j.jseaes.2004.11.002.

Dürr, S.B., 1996, Provenance of Xigaze fore-arc basin clastic rocks (Cretaceous, south Tibet): Geological Society of America Bulletin, v. 108, no. 6, p. 669–684, https://doi.org/10.1130/0016-7606(1996)108<0669:POXFAB>2.3.CO;2.

Duval, M., Bahain, J., Falgueres, C., Garcia, J., Guilarte, V., Grün, R., Martínez, K., Moreno , D., Shao, Q., and Voinchet, P., 2015, Revisiting the ESR chronology of the Early Pleistocene hominin occupation at Vallparadís (Barcelona, Spain): Quaternary International, v. 389, p. 213–223.

Einsele, G., Liu, B., Dürr, S., Frisch, W., Liu, G., Luterbacher, H., Ratschbacher, L., Ricken, W., Wendt, J., and Wetzel, A., 1994, The Xigaze forearc basin: Evolution and facies architecture (Cretaceous, Tibet): Sedimentary Geology, v. 90, no. 1, p. 1–32, https://doi.org/10.1016/0037-0738(94)90014-0.

Flament, N., Gurnis, M., Müller, R.D., Bower, D.J., and Husson, L., 2015, Influence of subduction history on South American topography: Earth and Planetary Science Letters, v. 430, p. 9–18, https://doi.org/10.1016/j.epsl.2015.08.006.

Garzanti, E., 2016, From static to dynamic provenance analysis—Sedimentary petrology upgraded: Sedimentary Geology, v. 336, p. 3–13, https://doi.org/10.1016/j.sedgeo.2015.07.010.

Garzanti, E., and Van Haver, T., 1988, The Indus clastics: Forearc basin sedimentation in the Ladakh Himalaya (India): Sedimentary Geology, v. 59, no. 3, p. 237–249, https://doi.org/10.1016/0037-0738(88)90078-4.

Gehrels, G., Kapp, P., DeCelles, P., Pullen, A., Blakey, R., Weislogel, A., Ding, L., Guynn, J., Martin, A., McQuarrie, N., and Yin, A., 2011, Detrital zircon geochronology of pre-Tertiary strata in the Tibetan-Himalayan orogen: Tectonics, v. 30, TC5016, https://doi.org/10.1029/2011TC002868.

Girardeau, J., Mercier, J., and Cao, Y., 1985a, Origin of the Xigaze ophiolite, Yarlung-Zangbo suture zone, southern Tibet: Tectonophysics, v. 119, n. 1–4, p. 407–433, https://doi.org/10.1016/0040-1951(85)90048-4.

Girardeau, J., Mercier, J., and Cao, Y., 1985b, Structure of the Xigaze ophiolite, Yarlung-Zangbo Suture Zone, southern Tibet, China: Genetic implications: Tectonics, v. 4, no. 3, p. 267–288, https://doi.org/10.1029/TC004i003p00267.

Göpel, C., Allègre, C.J., and Xu, R.-H., 1984, Lead isotopic study of the Xigaze ophiolite (Tibet): The problem of the relationship between magmatites (gabbros, dolerites, lavas) and tectonites (harzburgites): Earth and Planetary Science Letters, v. 69, no. 2, p. 301–310, https://doi.org/10.1016/0012-821X(84)90189-4.

Griffin, W., Pearson, N., Belousova, E.A., and Saeed, A., 2007, Reply to "Comment to short-communication 'Comment: Hf-isotope heterogeneity in zircon 91500' by W.L., Griffin, N.J. Pearson, E.A. Belousova and A. Saeed (Chemical Geology 233 (2006) 358–363)" by F. Corfu: Chemical Geology, v. 244, no. 1–2, p. 354–356, https://doi.org/10.1016/j.chemgeo.2007.06.023.

Hébert, R., Bezard, R., Guilmette, C., Dostal, J., Wang, C., and Liu, Z., 2012, The Indus–Yarlung-Zangbo ophiolites from Nanga Parbat to Namche Barwa syntaxes, southern Tibet: First synthesis of petrology, geochemistry, and geochronology with incidences on geodynamic reconstructions of Neo-Tethys: Gondwana Research, v. 22, no. 2, p. 377–397, https://doi.org/10.1016/j.gr.2011.10.013.

Hodges, K.V., 2000, Tectonics of the Himalaya and southern Tibet from two perspectives: Geological Society of America Bulletin, v. 112, no. 3, p. 324–350, https://doi.org/10.1130/0016-7606(2000)112<324:TOTHAS>2.0.CO;2.

Hu, X., Jansa, L., and Wang, C., 2008, Upper Jurassic–Lower Cretaceous stratigraphy in southeastern Tibet: Comparison with the western Himalayas: Cretaceous Research, v. 29, p. 301–315.

Hu, X., Jansa, L., Chen, L., Griffin, W.L., O'Reilly, S.Y., and Wang, J., 2010, Provenance of Lower Cretaceous Wölong Volcaniclastics in the Tibetan Tethyan Himalaya: Implications for the final breakup of Eastern Gondwana: Sedimentary Geology, v. 223, no. 3-4, p. 193–205, https://doi.org/10.1016/j.sedgeo.2009.11.008.

Hu, X., Garzanti, E., Moore, T., and Raffi, I., 2015, Direct stratigraphic dating of India-Asia collision onset at the Selandian (middle Paleocene, 59 ± 1 Ma): Geology, v. 43, no. 10, p. 859–862, https://doi.org/10.1130/G36872.1.

Hu, X., Garzanti, E., Wang, J., Huang, W., An, W., and Webb, A., 2016, The timing of India-Asia collision onset – Facts, theories, controversies: Earth-Science Reviews, v. 160, p. 264–299, https://doi.org/10.1016/j.earscirev.2016.07.014.

Hu, X., Wang, J., An, W., Garzanti, E., and Li, J., 2017, Constraining the timing of the India-Asia continental collision by the sedimentary record: Science China Earth Sciences, v. 60, no. 4, p. 603–625, https://doi.org/10.1007/s11430-016-9003-6.

Huang, W., van Hinsbergen, D.J.J., Maffione, M., Orme, D., Dupont-Nivet, G., Guilmette, C., Ding, L., Guo, Z., and Kapp, P., 2015, Lower Cretaceous Xigaze ophiolites formed in the Gangdese forearc: Evidence from paleomagnetism, sediment provenance, and stratigraphy: Earth and Planetary Science Letters, v. 415, p.142–153.

Ingersoll, R.V., Fullard, T.F., Ford, R.L., Grimm, J.P., Pickle, J.D., and Sares, S.W., 1984, The effect of grain size on detrital modes: A test of the Gazzi-Dickinson point-counting method: Journal of Sedimentary Research, v. 54, no. 1, p. 103–116.

Jackson, S.E., Pearson, N.J., Griffin, W.L., and Belousova, E.A., 2004, The application of laser ablation-inductively coupled plasma-mass spectrometry to in situ U–Pb zircon geochronology: Chemical Geology, v. 211, no. 1, p. 47–69, https://doi.org/10.1016/j.chemgeo.2004.06.017.

Jadoul, F., Berra, F., and Garzanti, E., 1998, The Tethys Himalayan passive margin from Late Triassic to Early Cretaceous (South Tibet): Journal of Asian Earth Sciences, v. 16, no. 2–3, p. 173–194, https://doi.org/10.1016/S0743-9547(98)00013-0.

Ji, W.-Q., Wu, F.-Y., Chung, S.-L., Li, J.-X., and Liu, C.-Z., 2009, Zircon U–Pb geochronology and Hf isotopic constraints on petrogenesis of the Gangdese batholith, southern Tibet: Chemical Geology, v. 262, no. 3–4, p. 229–245, https://doi.org/10.1016/j.chemgeo.2009.01.020.

Jin, X., Huang, H., Shi, Y., and Zhan, L., 2015, Origin of Permian exotic limestone blocks in the Yarlung-Zangbo Suture Zone, Southern Tibet, China: With biostratigraphic, sedimentary and regional geological constraints: Journal of Asian Earth Sciences, v. 104, p. 22–38, https://doi.org/10.1016/j.jseaes.2014.07.036.

Kochelek, E.J., Amato, J.M., Pavlis, T.L., and Clift, P.D., 2011, Flysch deposition and preservation of coherent bedding in an accretionary complex: Detrital zircon ages from the Upper Cretaceous Valdez Group, Chugach terrane, Alaska: Lithosphere, v. 3, no. 4, p. 265–274, https://doi.org/10.1130/L131.1.

Lash, G.G., 1985, Recognition of trench fill in orogenic flysch sequences: Geology, v. 13, no. 12, p. 867–870, https://doi.org/10.1130/0091-7613(1985)13<867:ROTFIO>2.0.CO;2.

Laurent, M., Falgueres, C., Bahain, J., Rousseau, L., and Van Vliet Lanoé, B., 1998, ESR dating of quartz extracted from quaternary and neogene sediments: Method, potential and actual limits: Quaternary Geochronology, v. 17, p. 1057–1062.

Leier, A.L., Kapp, P., Gehrels, G., and DeCelles, P.G., 2007, Detrital zircon geochronology of Carboniferous-Cretaceous strata in the Lhasa terrane, Southern Tibet: Basin Research, v. 19, p. 361–378, https://doi.org/10.1111/j.1365-2117.2007.00330.x.

Li, G., Sandiford, M., Boger, S., Liu, X., and Wei, L., 2015, Provenance of the Upper Cretaceous to Lower Tertiary sedimentary relicts in the Renbu Mélange Zone, within the Indus-Yarlung Suture Zone: The Journal of Geology, v. 123, no. 1, p. 39–54, https://doi.org/10.1086/680207.

Li, X.H., Wang, C.S., and Hu, X.M., 2005, Stratigraphy of deep-water Cretaceous deposits in Gyangze, southern Tibet, China: Cretaceous Research, v. 26, p. 33–41.

Li, Y., Wang, C., Hu, X., Bak, M., Wang, J., and Chen, L., 2007, Characteristics of Early Eocene radiolarian assemblages of the Saga area, southern Tibet and their constraint on the closure history of the Tethys: Chinese Science Bulletin, v. 52, p. 2108–2114, https://doi.org/10.1007/s11434-007-0302-1.

Liu, G., and Einsele, G., 1994, Sedimentary history of the Tethyan basin in the Tibetan Himalayas: Geologische Rundschau, v. 83, no. 1, p. 32–61, https://doi.org/10.1007/BF00211893.

Ludwig, K.R., 2011, Isoplot/Ex Version 4: A Geochronological Toolkit for Microsoft Excel: Geochronology Center, Berkeley, California, USA.

Malpas, J., Zhou, M.-F., Robinson, P.T., and Reynolds, P.H., 2003, Geochemical and geochronological constraints on the origin and emplacement of the Yarlung-Zangbo ophiolites, Southern Tibet, *in* Dilek, Y., and Robinson, P.T., eds., Ophiolites in Earth History: Geological Society London Special Publication 218, p. 191–206, https://doi.org/10.1144/GSL.SP.2003.218.01.11.

Matte, P., Mattauer, M., Olivet, J., and Griot, D., 1997, Continental subductions beneath Tibet and the Himalayan orogeny: A review: Terra Nova, v. 9, no. 5-6, p. 264–270, https://doi.org/10.1111/j.1365-3121.1997.tb00026.x.

Metcalf, K., and Kapp, P., 2017, The Yarlung suture mélange, Lopu Range, southern Tibet: Provenance of sandstone blocks and transition from oceanic subduction to continental collision: Gondwana Research, v. 48, p. 15–33, https://doi.org/10.1016/j.gr.2017.03.002.

Miall, A., 1978, Lithofacies types and vertical profile models in braided river deposits: A summary, *in* Miall A., ed, Fluvial Sedimentology: Canadian Society of Petroleum Geologists, Memoir 5, p. 597–604.

Mo, X., Niu, Y., Dong, G., Zhao, Z., Hou, Z., Zhou, S., and Ke, S., 2008, Contribution of syncollisional felsic magmatism to continental crust growth: A case study of the Paleogene Linzizong volcanic Succession in southern Tibet: Chemical Geology, v. 250, no. 1–4, p. 49–67, https://doi.org/10.1016/j.chemgeo.2008.02.003.

Mutti, E., 1992, Turbidite Sandstones: Azienda Generale Italiana Petroli, Parma, Italy, p. 275.

Mutti, E., and Ricci Lucchi, F., 1978, Turbidites of the northern Apennines: Introduction to facies analysis: International Geology Review, v. 20, no. 2, p. 125–166, https://doi.org/10.1080/00206817809471524.

Nilsen, T.H., and Zuffa, G.G., 1982, The Chugach Terrane, a Cretaceous trench-fill deposit, southern Alaska, *in* Leggett, J.K., ed., Trench-Forearc Geology: Sedimentation and Tectonics on Modern and Ancient Active Plate Margins: Geological Society of London Special Publication 10, no. 1, p. 213–227, https://doi.org/10.1144/GSL.SP.1982.010.01.14.

Orme, D.A., and Laskowski, A.K., 2016, Basin analysis of the Albian–Santonian Xigaze forearc, Lazi region, south-central Tibet: Journal of Sedimentary Research, v. 86, no. 8, p. 894–913, https://doi.org/10.2110/jsr.2016.59.

Orme, D.A., Carrapa, B., and Kapp, P., 2015, Sedimentology, provenance and geochronology of the Upper Cretaceous–Lower Eocene western Xigaze forearc basin, southern Tibet: Basin Research, v. 27, no. 4, p. 387–411, https://doi.org/10.1111/bre.12080.

Pan, G., Ding, J., Yao, D., and Wang, L., 2004, Geologic Map of the Qinghai-Xizang (Tibet) Plateau and adjacent areas, with guidebook: Chengdu, China, Chengdu Cartographic Publishing House, scale 1:1,500,000.

Pan, G., Mo, X., Hou, Z., Zhu, D., Wang, L., Li, G., Zhao, Z., Geng, Q., and Liao, Z., 2006, Spatial-temporal framework of the Gangdese orogenic belt and its evolution: Yanshi Xuebao, v. 22, no. 3, p. 521–533.

Ratschbacher, L., Frisch, W., Liu, G., and Chen, C., 1994, Distributed deformation in southern and western Tibet during and after the India-Asia collision: Journal of Geophysical Research: Solid Earth, v. 99, no. B10, p. 19917–19945, https://doi.org/10.1029/94JB00932.

Rink, W.J., Bartoll, J., Schwarcz, H.P., Shane, P., and Bar-Yosef, O., 2007, Testing the reliability of ESR dating of optically exposed buried quartz sediments: Radiation Measurements, v. 42, no. 10, p. 1618–1626, https://doi.org/10.1016/j.radmeas.2007.09.005.

Satur, N., Cronin, B., Hurst, A., Kelling, G., and Gürbüz, K., 2004, Down-channel variations in stratal patterns within a conglomeratic, deepwater fan feeder system (Miocene, Adana Basin, Southern Turkey) *in* Lomas, S.A., and Joseph, P., eds., Confined Turbidite Systems: Geological Society of London Special Publication 222, no. 1, p. 241–260, https://doi.org/10.1144/GSL.SP.2004.222.01.13.

Schärer, U., Xu, R.-H., and Allègre, C.J., 1984, U-Pb geochronology of Gangdese (Transhimalaya) plutonism in the Lhasa-Xigaze region, Tibet: Earth and Planetary Science Letters, v. 69, no. 2, p. 311–320, https://doi.org/10.1016/0012-821X(84)90190-0.

Scholl, D.W., and von Huene, R., 2007, Crustal recycling at modern subduction zones applied to the past—Issues of growth and preservation of continental basement crust, mantle geochemistry, and supercontinent reconstruction, *in* Hatcher, R.D., Carlson, M.P., McBride, J.H., Martínez Catalán, J.R., eds., 4-D Framework of Continental Crust: Geological Society of America Memoir 200, p. 9–32, https://doi.org/10.1130/2007.1200(02).

Sciunnach, D., and Garzanti, E., 2012, Subsidence history of the Tethys Himalaya: Earth Science Reviews, v. 111, p. 179–198, https://doi.org/10.1016/j.earscirev.2011.11.007.

Searle, M., Windley, B., Coward, M., Cooper, D., Rex, A., Rex, D., Tingdong, L., Xuchang, X., Jan, M., and Thakur, V., 1987, The closing of Tethys and the tectonics of the Himalaya: Geological Society of America Bulletin, v. 98, no. 6, p. 678–701, https://doi.org/10.1130/0016-7606(1987)98<678:TCOTAT>2.0.CO;2.

Sharman, G.R., Graham, S.A., Grove, M., Kimbrough, D.L., and Wright, J.E., 2015, Detrital zircon provenance of the Late Cretaceous–Eocene California forearc: Influence of Laramide low-angle subduction on sediment dispersal and paleogeography: Geological Society of America Bulletin, v. 127, no. 1–2, p. 38–60, https://doi.org/10.1130/B31065.1.

Shen, S., Dongli, S., and Shi, G.R., 2003a, A biogeographically mixed late Guadalupian (late Middle Permian) brachiopod fauna from an exotic limestone block at Xiukang in Lhaze county, Tibet: Journal of Asian Earth Sciences, v. 21, no. 10, p. 1125–1137, https://doi.org/10.1016/S1367-9120(02)00187-6.

Shen, S., Shi, G.R., and Archbold, N.W., 2003b, A Wuchiapingian (Late Permian) brachiopod fauna from an exotic block in the Indus–Tsangpo suture zone, southern Tibet, and its palaeobiogeographical and tectonic implications: Palaeontology, v. 46, no. 2, p. 225–256, https://doi.org/10.1111/1475-4983.00296.

Smith, G., Howell, D., and Ingersoll, R., 1979, Late Cretaceous trench-slope basins of central California: Geology, v. 7, no. 6, p. 303–306, https://doi.org/10.1130/0091-7613(1979)7<303:LCTBOC>2.0.CO;2.

Tapponnier, P., Mercier, J.L., Proust, F., Andrieux, J., Armijo, R., Bassoullet, J.P., Brunel, M., Burg, J.P., Colchen, M., Dupre, B., Girardeau, J., Marcoux, J., Mascle, G., Matte, P., Nicolas, A., Li, T., Xiao, X., Chang, C., Lin, B., Li, G., Wang, N., Chen, G., Han, T., Wang, X., Den, W., Zhen, H., Sheng, H., Cao, Y., Zhou, J., and Qiu, H., 1981, The Tibetan side of the India-Eurasia collision: Nature, v. 294, no. 5840, p. 405–410, https://doi.org/10.1038/294405a0.

Underwood, M.B., and Moore, G.F., 1995, Trenches and trench-slope basins, *in* Busby, C.J., and Ingersoll, R.V., eds., Tectonics of Sedimentary Basins: Cambridge, Massachusetts, USA, Blackwell Science, p. 179–220.

Walker, R.G., 1975, Generalized facies models for resedimented conglomerates of turbidite association: Geological Society of America Bulletin, v. 86, no. 6, p. 737–748, https://doi.org/10.1130/0016-7606(1975)86<737:GFMFRC>2.0.CO;2.

Wang, J., Hu, X., Jansa, L., and Huang, Z., 2011, Provenance of the Upper Cretaceous–Eocene deep-water sandstones in Sangdanlin, southern Tibet: Constraints on the timing of initial India-Asia Collision: The Journal of Geology, v. 119, p. 293–309, https://doi.org/10.1086/659145.

Wang, C., Li, X., Liu, Z., Li, Y., Jansa, L., Dai, J., and Wei, Y., 2012, Revision of the Cretaceous–Paleogene stratigraphic framework, facies architecture and provenance of the Xigaze forearc basin along the Yarlung-Zangbo suture zone: Gondwana Research, v. 22, no. 2, p. 415–433, https://doi.org/10.1016/j.gr.2011.09.014.

Wang, J., Hu, X., Garzanti, E., An, W., and Liu, X.-C., 2017a, The birth of the Xigaze forearc basin in southern Tibet: Earth and Planetary Science Letters, v. 465, p. 38–47, https://doi.org/10.1016/j.epsl.2017.02.036.

Wang, J., Hu, X., Garzanti, E., Ji, W., Liu, Z., Liu, X., and Wu, F., 2017b, Early cretaceous topographic growth of the Lhasaplano, Tibetan plateau: Constraints from the Damxung conglomerate: Journal of Geophysical Research: Solid Earth, v. 122, no. 7, p. 5748–5765, https://doi.org/10.1002/2017JB014278.

Wen, D.-R., Liu, D., Chung, S.-L., Chu, M.-F., Ji, J., Zhang, Q., Song, B., Lee, T.-Y., Yeh, M.-W., and Lo, C.-H., 2008, Zircon SHRIMP U–Pb ages of the Gangdese Batholith and implications for Neotethyan subduction in southern Tibet: Chemical Geology, v. 252, no. 3–4, p. 191–201, https://doi.org/10.1016/j.chemgeo.2008.03.003.

Willems, H., Zhou, Z., Zhang, B., and Gräfe, K.U., 1996, Stratigraphy of the upper cretaceous and lower tertiary strata in the Tethyan Himalayas of Tibet (Tingri area, China): Geologische Rundschau, v. 85, no. 4, p. 723–754, https://doi.org/10.1007/BF02440107.

Wu, F., Ji, W., Liu, C., and Chung, S., 2010, Detrital zircon U–Pb and Hf isotopic data from the Xigaze fore-arc basin: Constraints on Transhimalayan magmatic evolution in southern Tibet: Chemical Geology, v. 271, no. 1–2, p. 13–25, https://doi.org/10.1016/j.chemgeo.2009.12.007.

Wu, F., Ji, W., Wang, J., Liu, C., Chung, S., and Clift, P.D., 2014, Zircon U–Pb and Hf isotopic constraints on the onset time of India-Asia collision: American Journal of Science, v. 314, no. 2, p. 548–579, https://doi.org/10.2475/02.2014.04.

XBGMR, 1979, Regional Geology Report of the People's Republic of China: 1:1,000,000 (Xigaze H-45, Yadong G-45), Beijing, p. 230.

Yin, A., 2006, Cenozoic tectonic evolution of the Himalayan orogen as constrained by along-strike variation of structural geometry, exhumation history, and foreland sedimentation: Earth-Science Reviews, v. 76, p. 1–131, https://doi.org/10.1016/j.earscirev.2005.05.004.

Yin, A., and Harrison, T.M., 2000, Geologic evolution of the Himalayan-Tibetan orogen: Annual Review of Earth and Planetary Sciences, v. 28, no. 1, p. 211–280, https://doi.org/10.1146/annurev.earth.28.1.211.

Yin, J., Sun, Y., and Wen, C., 1988, Mesozoic stratigraphy from Dangla in Gyirong to Saga, southern Tibet: Journal of the Institute of Geology and Geophysics, Chinese Academy of Science, v. 3, p. 80–95.

Zheng, Y., Fu, Q., Hou, Z., Yang, Z., Huang, K., Wu, C., and Sun, Q., 2015, Metallogeny of the northeastern Gangdese Pb–Zn–Ag–Fe–Mo–W polymetallic belt in the Lhasa terrane, southern Tibet: Ore Geology Reviews, v. 70, p. 510–532, https://doi.org/10.1016/j.oregeorev.2015.04.004.

Zhu, J., Du, Y., Liu, Z., Feng, Q., Tian, W., Li, J., and Wang, C., 2005, Mesozoic radiolarian chert from the middle sector of the Yarlung-Zangbo suture zone, Tibet and its tectonic implications: Science in China Series D-Earth Sciences, v. 35, no. 12, p. 1131–1139.

Zhu, D., Pan, G., Chung, S., Liao, Z., Wang, L., and Li, G., 2008, SHRIMP Zircon Age and geochemical constraints on the origin of Lower Jurassic volcanic rocks from the Yeba Formation, southern Gangdese, south Tibet: International Geology Review, v. 50, no. 5, p. 442–471, https://doi.org/10.2747/0020-6814.50.5.442.

Zhu, D., Zhao, Z., Niu, Y., Mo, X., Chung, S., Hou, Z., Wang, L., and Wu, F., 2011, The Lhasa Terrane: Record of a microcontinent and its histories of drift and growth: Earth and Planetary Science Letters, v. 301, no. 1–2, p. 241–255, https://doi.org/10.1016/j.epsl.2010.11.005.

Zhu, D., Zhao, Z., Niu, Y., Dilek, Y., Hou, Z., and Mo, X., 2013, The origin and pre-Cenozoic evolution of the Tibetan Plateau: Gondwana Research, v. 23, no. 4, p. 1429–1454, https://doi.org/10.1016/j.gr.2012.02.002.

MANUSCRIPT RECEIVED 17 JULY 2017
REVISED MANUSCRIPT RECEIVED 31 DECEMBER 2017
MANUSCRIPT ACCEPTED 28 FEBRUARY 2018